IOP Publishing Physics in Medicine and Biology

Phys. Med. Biol. **52** (2007) 1659–1674 doi:10.1088/0031-9155/52/6/008

Perturbative diffusion theory formalism for interpreting temporal light intensity changes during laser interstitial thermal therapy

Lee C L Chin[1], **William M Whelan**[1,2] **and I Alex Vitkin**[1,3,4]

[1] Department of Medical Biophysics, University of Toronto and Ontario Cancer Institute, Toronto M5G 2M9, Canada
[2] Department of Physics, Ryerson University, Toronto M5B 2K3, Canada
[3] Department of Biophysics and Bioimaging, University of Toronto and Ontario Cancer Institute, Toronto M5G 2M9, Canada
[4] Department of Radiation Oncology, University of Toronto and Ontario Cancer Institute, Toronto M5G 2M9, Canada

E-mail: Lee.Chin@rmp.uhn.on.ca

Received 29 June 2006, in final form 8 January 2007
Published 26 February 2007
Online at stacks.iop.org/PMB/52/1659

Abstract

In an effort to understand dynamic optical changes during laser interstitial thermal therapy (LITT), we utilize the perturbative solution of the diffusion equation in heterogeneous media to formulate scattering weight functions for cylindrical line sources. The analysis explicitly shows how changes in detected interstitial light intensity are associated with the extent and location of the volume of thermal coagulation during treatment. Explanations for previously reported increases in optical intensity observed early during laser heating are clarified using the model and demonstrated with experimental measurements in *ex vivo* bovine liver tissue. This work provides an improved understanding of interstitial optical signal changes during LITT and indicates the sensitivity and potential of interstitial optical monitoring of thermal damage.

(Some figures in this article are in colour only in the electronic version)

1. Introduction

Interstitial point optical measurements are currently being explored for monitoring the location and dynamic extent of the coagulation volume during laser interstitial thermal therapy (LITT) (Chin *et al* 2001, 2003, 2004, Whelan *et al* 2005). During LITT, light energy is delivered directly into a solid tumour using thin, flexible optical fibres inserted interstitially usually under ultrasound guidance (Bown 1983). The emitted optical energy is scattered and absorbed, generating an increase in local temperature that results in coagulative necrosis of the tumour tissue at temperatures greater than ∼55 °C (Chung *et al* 1999, Hazle *et al* 2002). The ensuing

thermally induced structural changes result in dynamically changing optical, thermal and blood perfusion properties that make pre-treatment prediction of the final coagulation volume difficult. Hence, clinical implementation of LITT requires accurate monitoring techniques during the procedure to ensure complete destruction of the tumour while sparing healthy surrounding tissue. Magnetic resonance imaging (MRI) thermometry (McNichols *et al* 2004) has been demonstrated for monitoring LITT, but the technique is expensive, impractical in some clinical scenarios and unable to accurately visualize in real time the resulting structural damage. Alternatively, imaging of thermally induced property changes using computed tomography, MRI or ultrasound may provide a direct indicator of the coagulation extent (Amin *et al* 1993, Minhaj *et al* 2002, Bremer *et al* 2001, Malone *et al* 2004, Bevan and Sherar 2001). However, although these modalities have demonstrated promise for *post-treatment* verification of thermal damage, issues with imaging time and temperature-induced artefacts (i.e. non-structural enhancement due to temperature) currently restrict their on-line monitoring efficacy.

To address these limitations, recent research has focused on the potential of optical techniques for monitoring the extent of thermal coagulation during thermal therapies either by direct measurement of optical signal changes (Anderson *et al* 2004, Chin *et al* 2003, 2004, Terenji *et al* 2005) or by indirect measurement of opto-acoustic ultrasound signals (Larin *et al* 2005). This is because thermal coagulation results in significant changes in the optical properties of tissue—as evidenced by the changing visual appearance of meat as it cooks. In particular, the coagulated scattering properties have been shown to increase —two- to fourfold from the native state in some tissue types, thus providing an exceptional contrast between the two tissue states (Cheong 1995, Ritz *et al* 2001). Furthermore, optically based techniques are likely to be less sensitive to temperature artefacts that currently limit the on-line structural monitoring potential of MRI and ultrasound.

A number of initial studies have been performed to elucidate how changes in interstitially measured point optical signals can be used to gain information on the location and size of the coagulation volume. In particular, using Monte Carlo simulations and experiments in optical phantoms with thermally induced changes in optical properties, it has been shown that as thermal damage forms symmetrically around a source fibre, a decrease in light intensity is observed outside the coagulation zone whereas an increase in light intensity is measured inside the coagulation zone (see Roggan *et al* (2001) for an excellent description of the Monte Carlo simulation for LITT treatment planning). Hence, the detection of dynamic optical signals by implanted sensors can indicate the onset and growth of the coagulation zone (Chin *et al* 2003, 2004). These fundamental studies provide a simple but effective method of on-line optical monitoring of thermal damage during interstitial laser heating. However, the precise interpretation of these dynamic light intensity changes is lacking. For example, a previous work has demonstrated noticeable increases in interstitial optical intensity early during LITT of *ex vivo* bovine liver that occurs even when the coagulation boundary is far from the optical sensor (Chin *et al* 2001, Whelan *et al* 2005). One possible explanation of this change is photobleaching of absorbing tissue chromophores due to the high intensity of light (1–5 W) emitted during LITT (Chin *et al* 2001). This initial hypothesis was suggested from observations of dye photobleaching found in optical phantoms. However, it was not clear whether biological chromophores exhibit similar effects.

Here, we provide a simple interpretation of interstitial changes in light intensity (i.e. fluence) during LITT, using a perturbation model of the diffusion equation previously utilized for diffuse optical tomography of tissue. Although diffuse optical tomography also seeks to determine the location and volume of optical heterogeneities, a key difference is that during LITT, thermal lesion size changes dynamically, thereby providing additional temporal

optical information that may be used to infer the extent of the coagulated volume. However, interstitial optical monitoring typically measures light intensity at a single location, which makes interpretation of optical signal changes challenging.

In this work, the effect of localized scattering changes on temporally detected interstitial light intensities is investigated, and thus an explanation for the behaviour of measured optical fluence signals during LITT is presented.

2. Theory

2.1. Perturbative solution to the diffusion equation for a point source

Light propagation in turbid multiply scattering media such as tissues can be modelled using the diffusion equation (O'Leary 1996, Ostermeyer and Jacques 1997). In the case of heterogeneous media, the steady-state diffusion equation is

$$\nabla \cdot [D(\vec{r})\nabla U(\vec{r})] - \mu_a(\vec{r})U(\vec{r}) = -S(\vec{r}). \tag{1}$$

Here $U(\vec{r})$ is the photon fluence rate (or light intensity) (W cm^{-2}), $D(\vec{r}) \approx (3\mu_s'(\vec{r}))^{-1}$ is the diffusion coefficient (cm^{-1}), $\mu_s'(\vec{r})$ is the reduced scattering coefficient (cm^{-1}), $\mu_a(\vec{r})$ is the absorption coefficient (cm^{-1}) and $S(\vec{r})$ is the source term (W cm^{-3}). Here, the first-order similarity relation, $\mu_s' = \mu_s(1-g)$, combines the effects of the scattering coefficient, μ_s, and anisotropy factor, g, into a single parameter, μ_s', such that scattering can be considered as an isotropic process. The assumption that $D(\vec{r}) \approx (3\mu_s'(\vec{r}))^{-1}$ is generally valid because $\mu_a \ll \mu_s'$ for biological tissues at the near-infrared treatment wavelengths employed in LITT (Cheong 1995). Note that the tissue properties are a function of space to underscore the heterogeneous nature of the medium representing coagulated and native tissue. Here, we utilize a perturbation approach to solve equation (1) (Kak and Slaney 1988, O'Leary *et al* 1995, O'Leary 1996, Ostermeyer and Jacques 1997).

Performing the differentiation on the left-hand side of (1) using the chain rule results in

$$\nabla D(\vec{r}) \cdot \nabla U(\vec{r}) + D(\vec{r})\nabla^2 U(\vec{r}) - \mu_a(\vec{r})U(\vec{r}) = -S(\vec{r}). \tag{2}$$

The first term in (2) models the effects of scattering perturbations (Ostermeyer and Jacques 1997).

Equation (1) can further be expanded to first order by expressing the individual optical properties as a summation of a spatially varying and a background component:

$$\mu_a(\vec{r}) = \mu_{a0} + \delta\mu_a(\vec{r}),\ D(\vec{r}) = D_0 + \delta D(\vec{r}), \qquad \text{and} \qquad k^2 = -\frac{\mu_a(\vec{r})}{D(\vec{r})}.$$

Applying the above expansions and multiplying by $\frac{D_o}{D_o}$ gives

$$\left(\nabla^2 + F(\vec{r})k_o^2\right)U(\vec{r}) = -F(\vec{r})\left[\frac{S(\vec{r})}{D_o} + \frac{\delta\mu_a(\vec{r})}{D_o}U(\vec{r}) + \frac{\delta D(\vec{r})}{D_o}\nabla^2 U(\vec{r}) + \frac{\nabla\delta D(\vec{r})}{D_o}\cdot\nabla U(\vec{r})\right], \tag{3}$$

where $k_o^2 = -\frac{\mu_{ao}}{D_o}$.

The term $F(\vec{r}) = \frac{D_o}{D(\vec{r})} = \frac{\mu_s'(\vec{r})}{\mu_{s,o}'}$ is a scaling factor that accounts for changes in tissue scattering relative to the homogeneous background. When *only* absorption perturbations occur, $F(\vec{r}) \to 1$, but when scattering perturbations exist, the $F(\vec{r})$ term, which depends on the fractional change in scattering, must be included when calculating light intensity.

In the presence of heterogeneities ($\delta\mu_a(\vec{r})$, $\delta D(\vec{r})$), the total photon fluence can thus be expressed by a 'homogeneous' field $U_0(\vec{r})$, which is the photon fluence detected in a

homogeneous medium with properties μ_{a0} and D_0, and a 'perturbed' field, $U_{sc}(\vec{r})$, that results from the heterogeneities.

Ostermeyer and Jacques (1997) have solved equation (3) both numerically and analytically by employing a Born expansion. In this case, $U(\vec{r}) = U_o(\vec{r}) + U_{sc}(\vec{r})$ and the absolute fluence rate is determined. However, in most experimental situations, instead of the absolute fluence rate, a photovoltage proportional to the detected light intensity is measured. Furthermore, with interstitial thermal therapies, we are interested in the *change* in light intensity that results from thermal damage *relative* to the light intensity measured prior to heating. In such cases, absolute measurements are not required and we can express the fluence, $U(\vec{r})$, using the Rytov expansion (Kak and Slaney 1988, O'Leary 1996):

$$U(\vec{r}) = U_0(\vec{r})U_{sc}(\vec{r}) = U_0(\vec{r})\,e^{\phi_{sc}(\vec{r})}. \tag{4}$$

Here, the scattered light intensity, $U_{sc}(\vec{r})$, is expressed in terms of an exponential complex phase, $\phi_{sc}(\vec{r})$, and rearranging equation (4), $\ln\left(\frac{U(\vec{r})}{U_0(\vec{r})}\right) = \phi_{sc}(\vec{r})$, we immediately see that, unlike the Born expansion, we are only interested in the *relative* change in the optical signal due to a potential perturbation.

By substituting the expression for $U(\vec{r})$ (equation (4)) into equation (3) and expanding, an analytical solution for $\phi_{sc}(\vec{r})$ can be found by convolving equation (3) with Green's function, $G(\vec{r})$, for the geometry of interest. For simplicity, we will ignore the spatially dependent notation for the remainder of this derivation until the final form of the equation is presented.

In the case of both absorption and scattering perturbations in an infinite medium, the result is an integral equation:

$$\phi_{sc} = -\frac{1}{U_o}\int_{V\,obj} d^3\vec{r}\,F\left[\frac{\delta D}{D_o}GU_o(\nabla\phi_{sc})^2 - \frac{\delta D}{D_o}\nabla G\cdot\nabla U_o + GU_o(\nabla\phi_s)^2 + GU_o\frac{\delta\mu_a}{D_o}\right]. \tag{5}$$

Note that equation (5) is nonlinear as it expresses $\phi_{sc}(\vec{r})$ as a function of itself. To simplify the equation, we employ the Rytov approximation (Kak and Slaney 1988, O'Leary 1996). The basic assumption of the Rytov approximation is that the scattered light intensity is slowly varying such that (Kak and Slaney 1988, O'Leary 1996)

(1) $(\nabla\phi_{sc})^2 \ll \nabla G\cdot\nabla U_o$,
(2) $(\nabla\phi_{sc})^2 \ll \frac{\delta\mu_a}{D_o}$,
(3) $\frac{\delta D}{D_o} < 1$.

Application of the above assumptions to equation (5) results in the first-order perturbative Rytov solution (Kak and Slaney 1988, O'Leary 1996) of the heterogeneous diffusion equation for the scattered phase:

$$\phi_{sc} = -\frac{1}{U_o}\int_{V\,obj} d^3r\,F\left[-\frac{\delta D}{D_o}\nabla G\cdot\nabla U_o + GU_o\frac{\delta\mu_a}{D_o}\right]. \tag{6}$$

From the literature, the largest change in the reduced scattering coefficient resulting from thermal damage is on the order of ~2–4× yielding $\frac{\delta D}{D_o} \sim 0.75$ (Cheong 1995), which is expected to be within the requirements of the Rytov approximation. The quantitative limits of these assumptions as pertaining to interstitial optical monitoring of LITT are evaluated in the appendix, where it is demonstrated that the perturbative solution is accurate to within ~10% compared to an analytical diffusion theory model for typical tissue scattering changes and experimental geometries.

Employing the above assumptions and reintroducing the spatial dependence, the scattered phase, ϕ_{sc}, becomes the summation of source-detector dependent weights for both scattering, W_{sc}, and absorption, W_a, $\phi_{sc} = \sum\left(W_{sc}\frac{\delta D}{D_o} + W_a\frac{\delta\mu_a}{D_o}\right)$ where:

$$W_{sc} = \frac{F(\vec{r})\nabla G(|\vec{r}-\vec{r}_d|)\cdot\nabla U_o(\vec{r},\vec{r}_s)d^3\vec{r}}{U_o(\vec{r}_d,\vec{r}_s)} \tag{7}$$

is scaled by the local scattering $\left(\frac{\delta D}{D_o}\right)$ difference and:

$$W_a = -\frac{F(\vec{r})G(|\vec{r} - \vec{r}_d|)U_o(\vec{r}, \vec{r}_s)d^3\vec{r}}{U_o(\vec{r}_d, \vec{r}_s)} \tag{8}$$

is scaled by the local absorption $\left(\frac{\delta \mu_a}{D_o}\right)$ difference. In equations (7) and (8), $\vec{r}$ is the location of the perturbation, $\vec{r}_d$ is the location of the detector and $\vec{r}_s$ is the location of the source.

Due to the large increases in scattering that occur during LITT, we focus on only scattering perturbations (i.e. $\delta\mu_a(\vec{r}) = 0$). The right-hand side of equation (6) describes the relative contribution of the voxel at position $\vec{r}$, given a source positioned at $\vec{r}_s$ and a detector located at $\vec{r}_d$. A complete derivation has been previously reported (O'Leary 1996). The solution derived in this work yields a similar expression that differs only in presentation by the factor F. A similar factor was presented for the analytical expression to the Born expansion derived by Ostermeyer and Jacques (1997).

2.2. Modelling a line source with the perturbative solution of the diffusion equation

In the previous section, we derived the perturbative solution of the diffusion equation for a spherical point source. However, many LITT treatments employ cylindrical diffusers instead of spherical sources. To extend our model to the case of a finite line source, the scattered phase for a point source, ϕ_{sc}, described in equation (6) is integrated over the spatial extent of the cylindrical source:

$$\phi_{sc,line}(\vec{r}_{s,centre}, \vec{r}_d) = \frac{1}{L}\int_{\vec{r}_{s,centre-L/2}}^{\vec{r}_{s,centre+L/2}} \phi_{sc}(\vec{r}_s, \vec{r}_d)\, d\vec{r}. \tag{9}$$

Here $\vec{r}_{s,centre}$ is the location of the mid-point of the line source, $\vec{r}_d$ is the location of the detector, and L is the length of the line source (cm). A zero thickness is assumed for the fibre diffuser.

Numerical integration of equation (9) was performed using an adaptive Simpson quadrature routine in the Matlab V6 software package (Mathworks, Natich, Mass, USA). When $\vec{r} = \vec{r}_s$ or $\vec{r} = \vec{r}_d$, the weights go to infinity and cannot be described by equation (6). To account for these discontinuities, a self-interaction term has been proposed that provides a physical description of the weight at these positions (Ostermeyer and Jacques 1997). However, O'Leary *et al* (1995) had previously demonstrated that the effects of the self-interaction term are small. Furthermore, experimentally these positions are occupied by a finite sized source or detector and do not contribute to the attenuation properties of the medium. Therefore, for simplicity, we have set all such terms to zero.

3. Results and discussion

Figure 1 shows the scattering weights, W_{sc}, (equation (7)) as a function of position at the $z = 0$ cm plane for a 2 cm cylindrical diffuser centred at $(x, y) = (0, 0)$ cm and for a sensor located at $(x, y) = (+0.75, 0)$ cm. Here, the diffuser active length spans from $y = -1$ to 1 cm. Although the weights are displayed on a single plane, the model is three dimensional. The voxels utilized were $0.05 \times 0.05 \times 0.05$ cm^3 with the total spatial domain spanning $x = -2$ to 2 cm, $y = -2$ to 2 cm and $z = -2$ to 2 cm. The voxel size was chosen to ensure sufficient resolution while the spatial domain was selected to simulate an effectively infinite medium (i.e. the weight function values are $\sim$0 at the domain boundaries). The native optical properties were chosen to be $\mu_{a,o} = 0.5$ cm^{-1} and $\mu'_{s,o} = 10$ cm^{-1}, approximating those of porcine liver at 810 nm

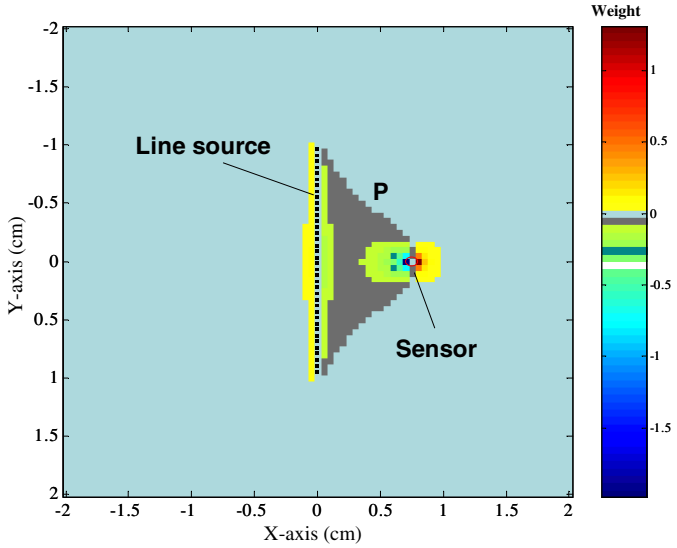

Figure 1. Scattering weight function, W_{sc}, at the $z = 0$ cm plane for a 2 cm cylindrical line source located at $x = 0$ cm and $y = -1$ to 1 cm. The sensor is located at $(x, y, z) = (+0.75, 0, 0)$ cm. The baseline (native) properties are $\mu_a = 0.5$ cm^{-1} and $\mu_s' = 10$ cm^{-1}. As shown by point P, scattering changes outside the direct line of sight between the source and sensor can also lead to fluence increases.

(Ritz *et al* 2001). Note that the coagulated, or perturbed, optical properties, $\delta\mu_a$ and $\delta\mu_s'$, do not play a role in the scattering weight matrices (e.g. the optical response to heterogeneities are solely determined by geometry and the native optical properties) and only determine the magnitude of the perturbed signal. Hence, while a quantitative agreement of our model results is not expected in all tissues, the qualitative response of the perturbed signal is expected to be comparable.

Figure 1 demonstrates that scattering perturbations can result in both increases and decreases in detected fluence depending on the location of the heterogeneities. Increases in scattering to the left of the source (negative x values) or to the right of the sensor (greater than $x = 0.75$ cm) can result in increases in fluence (positive weights). Conversely, scattering increases directly between the source and sensor result in decreases in fluence (negative weights). Interestingly, outside the direct line of sight between the source and the sensor (as indicated by point P in figure 1), scattering changes can also lead to fluence increases. The greatest effects occur within the vicinity of the sensor because all photons that reach the sensor position must pass through these regions to be detected. Outside the line of sight, figure 1 also indicates that at radial positions greater than ~0.5 cm from either the source or the sensor, changes in scattering would result in virtually no effect on the detected optical signal because the probability of such photons passing through these positions and being detected is negligible. As the thermal lesion evolves, a combination of increases and decreases in fluence may be detected depending on the overall shape of the coagulation boundary. Hence, the optical response to coagulation formation is complex and may be difficult to interpret depending on the symmetry, source-detector positions and location of the coagulation volume.

To illustrate this complexity, we present three cases for two sensors located at $(x, y) = (-0.75, 0)$ cm and $(+0.75, 0)$ cm, respectively. Here the native scattering is $\mu_{s,o}' = 10$ cm^{-1} with the introduced perturbations $1.5\times$ ($\mu_s' = 15$ cm^{-1}), $2\times$ ($\mu_s' = 20$ cm^{-1}) and $3\times$ ($\mu_s' = 30$ cm^{-1}) $\mu_{s,o}'$. A $3\times$ increase in scattering is typical of liver tissue (Ritz *et al* 2001). In all

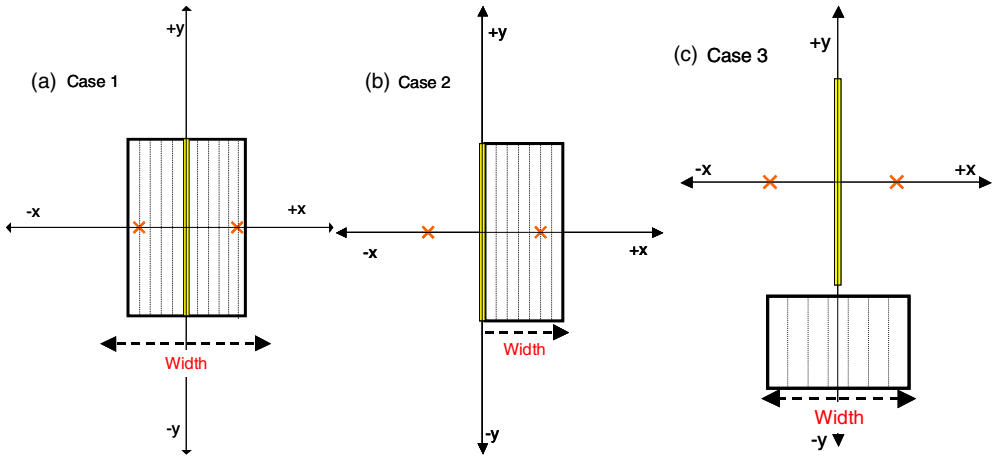

Figure 2. Case geometries for a growing scattering perturbation around a 2 cm line source: (a) coagulation formation symmetric about $(x, y) = (0, 0)$ cm and with growth in the positive and negative x directions, (b) asymmetric coagulation formation, symmetric about $y = 0$ cm with growth in the positive x direction only and (c) asymmetric coagulation formation symmetric about $(x, y) = (0, -1.2)$ cm with growth in the positive and negative x directions. The solid rectangles represent the regions of increased scattering corresponding to LITT-induced thermal lesions. The symbols are sensor (red cross), source (yellow rectangle) and scattering perturbation (solid rectangle). Each dashed line in the scattering perturbation rectangle indicates a different coagulation size. The coagulation grows along the x-axis.

cases, a constant $\mu_a = 0.5\ \text{cm}^{-1}$ was assumed. The geometries of the three cases are illustrated in figure 2.

In the first case (figure 2(a)), a rectangular scattering perturbation is introduced centred at $(x, y) = (0, 0)$ cm and with constant length between $y = -1$ and 1 cm. The resulting change in light intensity due to the scattering perturbation is calculated as the perturbation width increases symmetrically in the negative and positive x and z directions up to -1 and 1 cm, respectively.

Figure 3 demonstrates that as the perturbation (coagulation) boundary grows towards the $x = \pm 0.75$ cm sensor, a decrease in fluence occurs due to the increase in scattering, which acts to trap the light within the region of coagulation. Physically, this light trapping effect is associated with a higher number of scattering events within the region of coagulation, causing more local deposition of energy within the coagulated region and less energy deposition outside the coagulated region. As the perturbation (coagulation) boundary passes the sensor and continues to grow, the light trapping effect results in a slight increase in fluence as the scattering perturbation boundary increases past the sensor location. The same trends are seen for all three μ_s' changes investigated, with the features becoming more pronounced as μ_s' increases. Therefore, when symmetric coagulation formation occurs during LITT, dynamic fluence changes may signal the onset (initial decrease), approach (further decrease) and passing (increase) of the coagulation boundary. In a typical LITT treatment, the coagulation width (volume) is expected to grow during the course of the treatment. As such, the x-axis in figure 3 is also representative of the 'heating time'. Such observations have been previously reported by our group, both experimentally and using Monte Carlo models for spherical and cylindrical geometries (Chin *et al* 2003, 2004).

We now illustrate how asymmetric coagulation formation complicates the interpretation of relative fluence data.

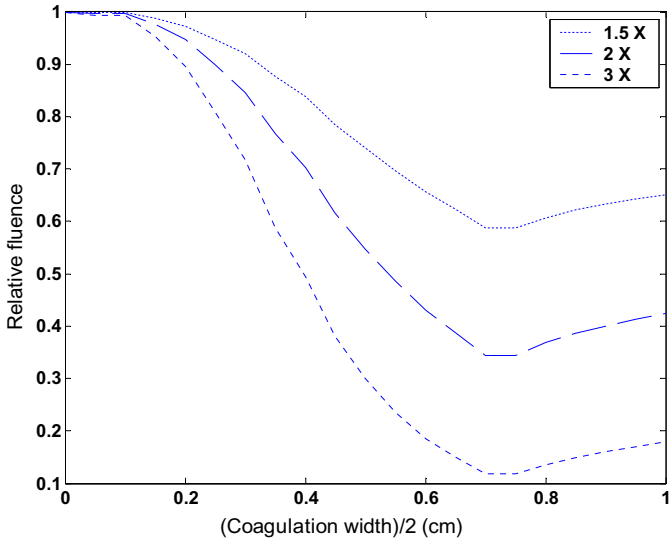

Figure 3. Relative change in fluence at $(x, y) = (\pm 0.75, 0)$ cm due to an increasing coagulation width as described in case 1 (figure 2(a)). Here, the coagulation width increases symmetrically about the y-axis. The perturbed (coagulated) optical properties are $\mu_a = 0.5\ \text{cm}^{-1}$ and $\mu_s' = 15, 20$ and $30\ \text{cm}^{-1}$ corresponding to a $1.5\times$, $2\times$ and $3\times$ increase in μ_s'. The relative fluence decreases significantly prior to passing of the perturbation (coagulation) boundary and increases after passage of the boundary. Since the coagulation width is expected to increase during LITT, the x-axis is also representative of treatment time.

Figure 2(b) demonstrates one such case whereby a rectangular scattering perturbation symmetric about the x-axis with constant length between $y = -1$ and 1 cm increases in width *only* in the positive x direction up to $x = +1$ cm. Again, the coagulation size increases symmetrically in the z direction up to -1 and 1 cm as the width increases in the x direction. In this case, the $(x, y, z) = (-0.75, 0, 0)$ cm sensor detects a steady increase in fluence as the perturbation (coagulation) volume increases. Conversely, the $(x, y, z) = (+0.75, 0, 0)$ cm sensor detects a steady decrease in fluence followed by a slight increase in fluence as the perturbation volume passes the sensor position. The trends for both sensor positions are magnified with an increasing scattering change. Therefore, unlike the symmetric case, early increases in fluence detected during LITT may not indicate passing of the coagulation boundary but, instead, may result from asymmetries in lesion formation. Such asymmetries may be due to asymmetric emission patterns in the cylindrical source fibre (Bremer *et al* 2001, Puccini *et al* 2003, Davidson *et al* 2005) or from cooling effects due to the presence of large vessels in the vicinity of the light source (Whelan *et al* 1995, Verhey *et al* 2003).

Note that, to clearly demonstrate the effects of asymmetry, we have assumed in case 2 that the coagulation boundary grows preferentially on one side of the source *only* (e.g. unilateral asymmetry). However, for typical LITT experiments *in vivo*, asymmetries will generally even out due to heat conduction over the course of a treatment. The end result is a temporal change in light intensity that is a combination of the trends at $(x, y, z) = (-0.75, 0, 0)$ and $(x, y, z) = (+0.75, 0, 0)$ cm and/or an overall smaller change in light intensity relative to the unilateral case. To provide an indication of how the optical signal would change in such a situation, we repeated the simulation of case 2 except with the addition of a small region of coagulation, ranging from 0.05 to 0.15 cm, on the negative x side of the source fibre. The results are shown in figure 4(b) where it can be seen that compared to the unilateral case (0 cm) the overall

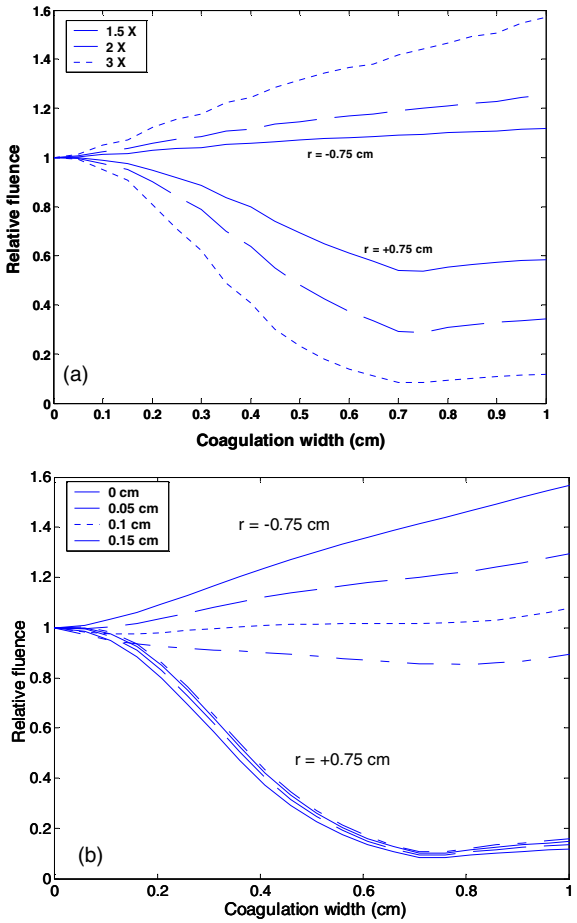

Figure 4. (a) Relative change in fluence at $(x, y, z) = (-0.75, 0, 0)$ cm and $(x, y, z) = (+0.75, 0, 0)$ cm due to an increasing coagulation width as described in case 2 (figure 2(b)). Here, the coagulation width increases asymmetrically relative to the y-axis in the positive x direction. The perturbed (coagulated) optical properties are $\mu_a = 0.5$ cm^{-1} and $\mu_s' = 15$, 20 and 30 cm^{-1} corresponding to a $1.5\times$, $2\times$ and $3\times$ increase in optical scattering. The fluence decreases prior to passing of the perturbation (coagulation) boundary and increases after passage of the boundary at the (+0.75, 0, 0) cm position (towards the coagulation side), but increases continuously at the $(-0.75, 0, 0)$ cm location (away from the coagulation side). (b) Same as the $3\times$ optical scattering case except an additional perturbation of 0.05 cm, 0.1 cm and 0.15 cm is now present on the negative x-axis side to simulate the potential experimental case of non-unidirectional asymmetries. The 0 cm case is equivalent to the $3\times$ case of figure 4(a).

magnitude of the light intensity changes for the $(x, y, z) = (-0.75, 0, 0)$ cm sensor decreases significantly as the region of coagulation on the negative x side increases. In fact, for a 0.15 cm width, an overall light intensity decrease is observed. This reason for this behaviour is that the negative weights for the $(x, y, z) = (-0.75, 0, 0)$ cm sensor (on the $-x$ side) dominate the positive weights (on the $+x$ side) of the sensor. This is emphasized by the virtually negligible influence that the added perturbation has on the light intensity changes for the $(x, y, z) = (+0.75, 0, 0)$ cm sensor where the corresponding positive weights are small.

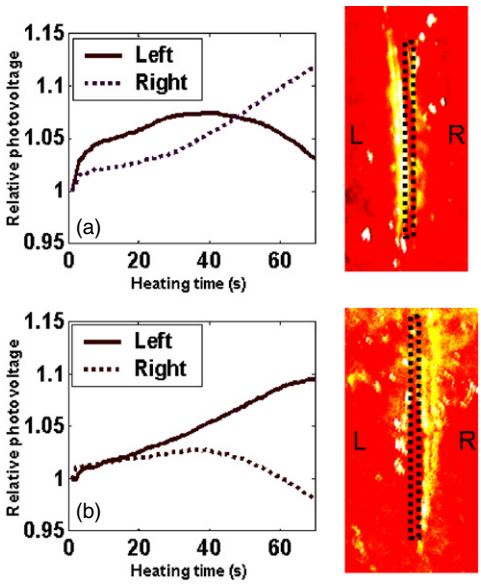

Figure 5. Experimental demonstration of scattering-induced increases in relative fluence during LITT in *ex vivo* bovine liver at 6 W. The applicator is a 2 cm diffuser with sensors positioned radially ∼0.75 cm from the centre of the cylindrical diffuser (dashed box) at the position of the L, R letters in the figure. The signal changes are a combination of those observed in the perturbation model of case 2. Relative fluence changes are shown for two separate experiments demonstrating optical signals measured (a) before and (b) after 180° rotation of the line source. The rotation results in a reversal of the optical signal trends at the same sensor locations. Contrast-enhanced gross photos also demonstrate that the coagulation asymmetry is reversed due to the fibre rotation (the white area is the coagulation).

We have experimentally observed the combination of light intensity changes typical of case 2, whereby two light sensors are positioned at opposite sides and at radial positions of ∼0.75 cm to the left and right from the centre of the active length of a 2 cm diffuser (Resonance Optics, MA, USA). The light sensors are connected to a photomultiplier tube, with the relative fluence read via a data acquisition card that averages ∼40 signals per second. These readings are displayed dynamically during heating. The fibres were sandwiched between two $6 \times 6\,\mathrm{cm}^2$ (x–y dimensions) and 3 cm thick slabs of fresh bovine liver (Whelan *et al* 2005). We note that differences in predicted light intensity may arise due to variations in optical properties from porcine (employed in our calculations) and bovine liver. However, we note that the perturbative formulation models light intensity changes due to *relative* changes in optical properties from baseline and will minimize differences in baseline absorption from individualized samples. In addition, the scattering weight functions maintain the same overall qualitative appearance regardless of baseline optical properties. Hence, while exact quantitative agreement is difficult, we expect that the qualitative change in light intensity will be well predicted. LITT was performed at 6 W for up to ∼100 s. The chosen LITT fibre had a characteristic polar asymmetry in the light emission pattern that resulted in slight asymmetries in the generated coagulation volumes at short heating times (∼70 s at 6 W).

Following heating the slabs were separated and a macroscopic photograph taken of the coagulated area. Figure 5(a) demonstrates a typical result along with an accompanying gross photograph. Increases in scattering are typically associated with coagulation, which manifests as a whitening upon gross macroscopic inspection (Pearce and Thomsen 1995).

The photograph has been contrast enhanced and the brightness adjusted to provide a clearer image of the induced coagulation.

Initially, the right-side sensor detects an increase in photovoltage while the left-side sensor detects a slight increase and subsequent decrease in photovoltage. A second experiment was conducted with the source rotated 180°, and the observed optical trends were reversed (figure 5(b)). As stated above, the coagulation asymmetries are not as pronounced as those shown in figure 2(b). This is likely due to two reasons. First, due to slight differences in the optical properties of porcine and bovine liver, we do not expect an exact quantitative agreement of the experimental measurements with the simulated perturbation results. Second, unlike the static models presented above, under experimental conditions the coagulation asymmetry causes the light intensity distribution to gradually 'shift' (and thereby cause an increase in heating) towards the uncoagulated side and dynamically balance the lesion asymmetry at longer heating times. Furthermore, although a coagulation asymmetry is visually observed at the source-sensor plane, small additional asymmetries may occur above or below this plane. This may explain the increase in signal experienced by all sensors early during heating ($<$40 s).

It should be noted that if photobleaching is the source of the light intensity increase as previously hypothesized (Chin *et al* 2001), an opposite trend is expected to occur whereby the sensor on the side closest to the asymmetric coagulation would experience an increase in light intensity. Therefore, while the purported photobleaching explanation may apply in phantoms where naphthol green dye is used as an absorber, the scattering asymmetry argument is the more likely explanation for the observed tissue fluence behaviour.

Finally, we present a third scenario (case 3 in figure 2(c)) whereby a rectangular scattering perturbation is centred about $(x, y, z) = (0, -0.7, 0)$ cm with a constant length of 0.6 cm (along the y-axis). Here, we calculate the resulting change in fluence due to the scattering heterogeneity as the perturbation width increases symmetrically in the negative and positive x and z directions up to x or $z = -1$ and 1 cm. As shown in figure 6, an immediate increase in fluence is observed at $(x, y, z) = (\pm 0.75, 0, 0)$ cm. Again, we observe that greater scattering changes result in more pronounced increases. The overall magnitude of the increase is much less than the $(x, y, z) = (-0.75, 0, 0)$ cm sensor in case 2 (figure 2(b)). This is because in these outer perturbation regions, the probability of photons reaching the detector that experienced the effect of the coagulation volume is much smaller than in regions close to the source. Once again, the implication is that small increases in fluence can occur without being caused by the coagulation boundary reaching the sensor position, and without photobleaching (i.e. decrease in μ_a).

The results of this work potentially clarify an increase in fluence during LITT previously attributed solely to photobleaching of chromophores (Chin *et al* 2001). Although absorption changes (reductions) are still a potential source of this fluence increase, we have shown here that scattering changes in asymmetric geometry may also result in early increases in detected interstitial fluence during optical heating.

Furthermore, the results of this work provide a potential framework for interpreting point optical signal changes during LITT. Under ideal conditions, optical sensors could be positioned at clinical margins where coagulation is desired, with the treatment terminated following a detected increase in light intensity. However, we have shown through theory and demonstrated in experiment that increases in light intensity can, in fact, result when asymmetries in coagulation formation occur around the heating source. Thus, a treatment control/termination strategy based on dynamic fluence measurements alone may be in error. One potential method for resolving such complications is to include a temperature sensor at the same location as the optical sensor. For example, when increases in optical signal occur early

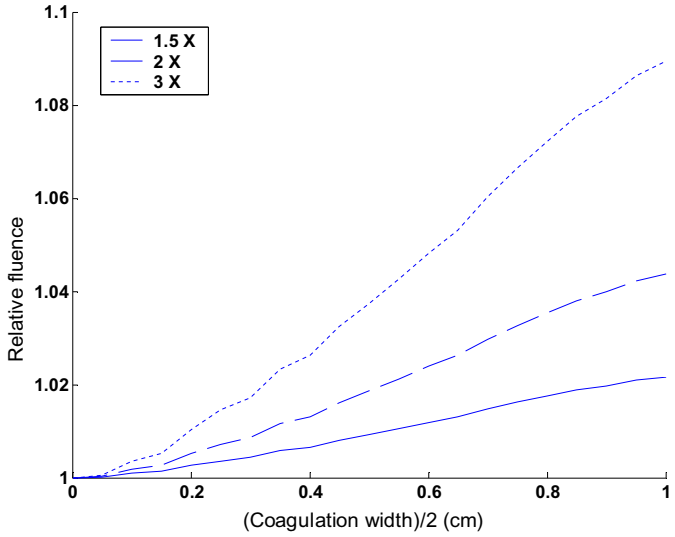

Figure 6. Relative change in fluence at $(x, y, z) = (\pm 0.75, 0, 0$ cm) due to increasing coagulation width as described in case 3 (figure 2(c)). Here, the coagulation width increases symmetrically about the y-axis. The perturbed (coagulated) optical properties are $\mu_a = 0.5$ cm^{-1} and $\mu_s' = 15$, 20 and 30 cm^{-1} corresponding to a 1.5×, 2× and 3× increase in optical scattering. The fluence increases continuously as the perturbation volume increases.

during LITT, a measured temperature below ∼55 °C (the approximate coagulation threshold temperature for rabbit thigh (Cheng *et al* 2003)) at the same location may indicate the presence of coagulation asymmetries either from asymmetric fibre emission (Bremer *et al* 2001, Puccini *et al* 2003, Davidson *et al* 2005) and/or cooling due to the presence of large blood vessels (Whelan *et al* 1995). Conversely, a measured temperature above ∼55 °C coupled with a detected fluence increase would aid in verifying the passing of the coagulation boundary.

Finally, we note that in its current implementation, the perturbative diffusion theory model allows one to better interpret the optical signal behaviour of point optical measurements under different geometries and coagulation asymmetries that may occur during LITT. However, such interpretation would require significant expertise as the point optical signal is the integrated contribution of thermal damage over all three-dimensional space. A potential approach for alleviating such complex interpretations may be the acquisition of multiple optical data points at different spatial locations to produce optical scattering profiles. Traditionally, perturbation methods have been utilized for optical tomographic reconstructions using non-invasive sources and detectors placed on the surface of tissues (Ntziachristos *et al* 2000). A combination of interstitial scanning sources and sensors along with suitable diffuse optical reconstruction techniques based on the perturbation model presented here may allow an estimation of the coagulation volume along a single plane. Since thermal coagulation results in optical property changes independent of heating modality, such a technique may also be applied to monitoring non-optical interstitial thermal therapies including microwave and ultrasound.

Acknowledgments

The authors would like to thank Arthur Worthington of Ryerson University for experimental assistance. This work was supported by the National Cancer Institute of Canada (with funds from the Canadian Cancer Society) and the Natural Sciences and Engineering Research Council of Canada.

Appendix. Comparison of perturbative solution with analytical two-region spherical diffusion theory

Although the primary goal of this work was to assess general (qualitative) trends in internal light fluence due to regions of varying scattering at interstitial locations around a cylindrical emitting light source, we briefly evaluate the quantitative performance of the perturbation model. Previous studies have examined the quantitative performance of the perturbation model for non-invasive imaging (O'Leary 1996). However, interstitial optical monitoring is performed under experimental conditions different than conventional diffuse optical tomography (DOT). In particular, the primary differences between the two techniques are as follows.

(i) The source in conventional DOT is typically located outside of the heterogeneity (i.e. on the surface of the background medium) while the source can be contained within the heterogeneity during interstitial optical monitoring.

(ii) Unlike conventional OT, in the interstitial setting, the detector is often located close to the source and inside or near the object boundary.

(iii) The scattering contrasts for coagulated heterogeneities is much larger than those expected for diagnostic DOT applications.

To our knowledge, previous publications have not evaluated the quantitative performance of the perturbation model under interstitial conditions. Therefore, we now compare our results from the perturbation model to an analytical two-region diffusion theory expression (approximating a spherical region of fully coagulated tissue surrounded by native tissue) for a point source (Iizuka *et al* 2000).

Figure 7(a) shows a quantitative comparison of the expected changes in fluence at $r = 0.75$ cm predicted by a two-region spherical diffusion theory (2-R SDT) solution and the perturbation solution to the diffusion equation that result from an increasing spherical inhomogeneity. Note that the analytical 2-R SDT does not employ the assumptions of the Rytov approximation and, therefore, provides a means to assess the inaccuracies of the perturbation solution. Here, the native optical properties were chosen to be $\mu_a = 0.5$ cm^{-1} and $\mu_s' = 10$ cm^{-1}. Changes in μ_s' for the resulting spherical perturbation were examined for 1.5, 2, 3 and 4$\times$ the native value. The voxels utilized were $0.05 \times 0.05 \times 0.05$ cm^3 with the total spatial domain spanning $x = -2$ to 2 cm, $y = -2$ to 2 cm and $z = -2$ to 2 cm. The source is located at the centre of the inhomogeneity with the optical properties the same as those stated above in the primary text. The voxel resolution was chosen to provide sufficient resolution to ensure a smooth fluence change as a function of coagulation radius. When lower resolution voxels are utilized, some artefacts begin to arise that are due to the discrete nature of the cubic voxels.

Several interesting observations are made regarding figure 7(a). First, as expected from assumption 1 (and 2) of the Rytov approximation, the most significant disagreement occurs when the coagulation boundary is close to the sensor position, with the error increasing as the boundary approaches the sensor position and decreasing after passing the sensor position. This disagreement is expected of the Rytov approximation which performs poorly when the photon field changes rapidly. In particular, because the 2-R SDT models a sharp boundary with exact boundary conditions the disagreement between the two models is particularly pronounced. Figure 7(b) shows the discrepancy between the two models as a function of coagulation radius. The discrepancy typically remains below $\sim$10% when the boundary is greater than $\sim$0.25 cm from the sensor position although the perturbation model appears to recover rapidly following the passing of the coagulation boundary. This is likely because when the sensor is

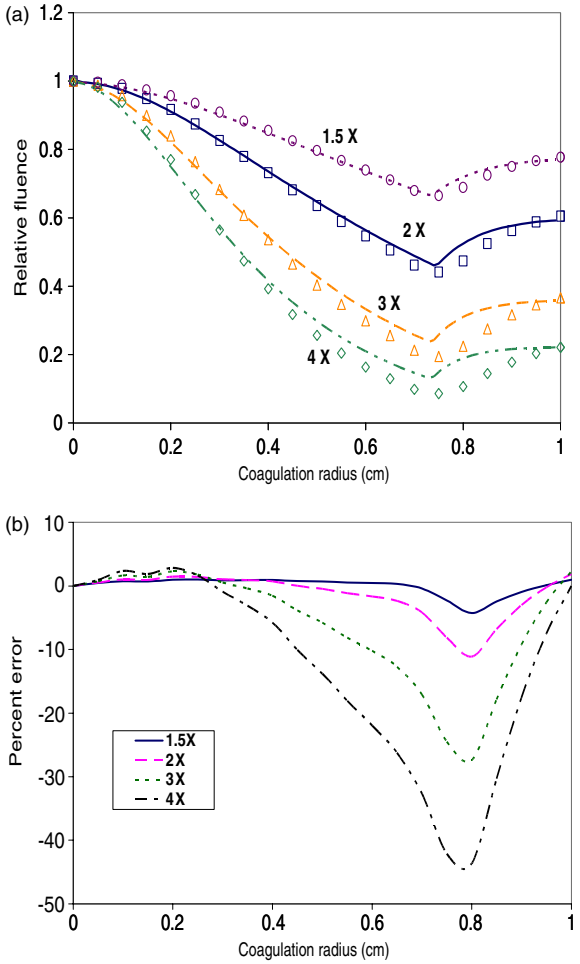

Figure 7. (a) A comparison of relative fluence change as a function of coagulation radius at $r = 0.75$ cm predicted by an analytical two-region spherical diffusion theory model (Iizuka *et al* 2000, solid lines) and a perturbative solution (this paper, symbols) to the diffusion equation. The native optical properties are $\mu_a = 0.5$ cm^{-1} and $\mu_s' = 10$ cm^{-1} while the perturbed (coagulated) optical properties are $\mu_a = 0.5$ cm^{-1} with μ_s' of 1.5×, 2×, 3×, and 4× the native μ_s'. The largest disagreement occurs for larger scattering changes and when the coagulation boundary is close to the detector position. (b) Per cent discrepancy between an analytical two-region spherical diffusion theory model and a perturbative solution to the diffusion equation. The greatest disagreement occurs for large changes in scattering (3–4×) and when the coagulation boundary is near the vicinity of the sensor located at $r = 0.75$ cm.

located within the perturbation, the fluence field decays more rapidly compared to outside the perturbation, thereby minimizing the effects of the boundary.

Second, figures 7(a) and (b) demonstrate that, as expected from assumption 3 of the Rytov approximation, the discrepancy at the boundaries increases as the scattering changes increase. This is because larger scattering changes result in more rapidly changing fluence fields. For scattering changes less than ∼2×, deviations remain below ∼10% but increase to almost 40% as the scattering increases to 4× deviations. However, regardless of the scattering

change, agreements are typically within 10% provided the boundary is greater than 0.3 cm from the sensor location. In the main body of this paper we performed studies where small asymmetries in coagulation formation were observed around an interstitial line source. In these experiments, scattering changes were approximately 3× the native tissue scattering while optical sensors were located 5 mm or greater from the coagulation boundary. Hence, based on the results of this appendix, we can expect the perturbative model to predict relative change in light intensity (measured during experiments) to an accuracy better than ∼5%.

This paper concentrates on the general trends in predicted light intensity due to asymmetries in coagulation formation around an interstitial line source. Scattering changes no greater than 3× are examined with the boundary of the asymmetries, typically 5 mm or greater from the sensor location. Under these conditions, we can expect the perturbative model to predict the relative change in light intensity with accuracy better than ∼5%.

Finally, we note that although the qualitative nature of the 2-R SDT and perturbative models is similar, quantitatively, the perturbative solution underestimates the true light intensity for geometries typical of interstitial laser heating. This has important implications if the perturbative model is to be applied to interstitial optical tomography of tissue scattering changes due to thermal coagulation, where it may result in a significant underestimation of the true scattering change. How and if such quantitative inaccuracies will lead to spatial reconstruction errors of the boundary location will be the subject of future investigation.

References

Amin Z, Thurrell W, Spencer G M, Harries S A, Grant W E, Bown S G and Lees W R 1993 Computed tomography-pathologic assessment of laser-induced necrosis in rat liver *Invest. Radiol.* **28** 1148–54

Anderson C D, Lin W C, Buttemere C R, Washington M K, Mahadevan-Jansen A, Pierce J, Nicoud I B, Pinson C W and Chari R S 2004 Real-time spectroscopic assessment of thermal damage: implications for radiofrequency ablation *J. Gastrointest. Surg.* **8** 660–9

Bevan P D and Sherar M D 2001 B-scan ultrasound imaging of thermal coagulation in bovine liver: frequency shift attenuation mapping *Ultrasound Med. Biol.* **27** 809–17

Bown S G 1983 Phototherapy in tumors *World J. Surg.* **7** 700–9

Bremer C, Kreft G, Roggan A, Filler T and Reimer P 2001 Ex vivo evaluation of novel miniaturized laser-induced interstitial thermotherapy applicators for effective small-volume tissue ablation *Invest. Radiol.* **36** 327–34

Cheng H L M, Purcell C M, Bilbao J M and Plewes D B 2003 Prediction of subtle thermal histopathological change using a novel analysis of Gd-DTPA kinetics *J. Magn. Reson. Imaging* **18** 585–98

Cheong W F 1995 Summary of optical properties *Optical-Thermal Response of Laser-Irradiated Tissue* ed A J Welch and M J C van Gemert (New York: Plenum) pp 275–303 (Appendix to Chapter 8)

Chin L C L, Whelan W M, Sherar M D and Vitkin I A 2001 Changes in relative light fluence measured during laser heating: implications for optical monitoring and modelling of interstitial laser photocoagulation *Phys. Med. Biol.* **46** 2407–20

Chin L C L, Whelan W M and Vitkin I A 2003 Models and measurements of light intensity changes during laser interstitial thermal therapy: implications for optical monitoring of the coagulation boundary location *Phys. Med. Biol.* **48** 543–59

Chin L C L, Wilson B C, Whelan W M and Vitkin I A 2004 Radiance-based monitoring of the extent of tissue coagulation during laser interstitial thermal therapy *Opt. Lett.* **29** 959–61

Chung A H, Jolesz F A and Hynynen K 1999 Thermal dosimetry of a focused ultrasound beam in vivo by magnetic resonance imaging *Med. Phys.* **26** 2017–26

Davidson S R, Vitkin I A, Sherar M D and Whelan W M 2005 Characterization of measurement artefacts in fluoroptic temperature sensors: implications for laser thermal therapy at 810 nm *Lasers Surg. Med.* **36** 297–306

Hazle J D, Stafford R J and Price R E 2002 Magnetic resonance imaging-guided focused ultrasound thermal therapy in experimental animal models: correlation of ablation volumes with pathology in rabbit muscle and VX2 tumors *J. Magn. Reson. Imaging* **15** 185–94

Iizuka M N, Vitkin I A, Kolios M C and Sherar M D 2000 The effects of dynamic optical properties during interstitial laser photocoagulation *Phys. Med. Biol.* **45** 1335–57

Kak A C and Slaney M 1988 *Principles of Computerized Tomographic Imaging* (New York: IEEE)

Larin K V, Larina I V and Esenaliev R O 2005 Monitoring of tissue coagulation during thermotherapy using optoacoustic technique *J. Phys. D: Appl. Phys.* **38** 2645–53

Malone D E, Wyman D R, DeNardi F G, McGrath F P, De Gara C J and Wilson B C 1994 Hepatic interstitial laser photocoagulation. An investigation of the relationship between acute thermal lesions and their sonographic images *Invest. Radiol.* **29** 915–21

McNichols R J, Gowda A, Kangasniemi M, Bankson J A, Price R E and Hazle J D 2004 MR thermometry-based feedback control of laser interstitial thermal therapy at 980 nm *Lasers Surg. Med.* **34** 48–55

Minhaj A M, Mann F, Milne P J, Denham D B, Salas N Jr, Nose I, Damgaard-Iversen K, Parel J M and Robinson D S 2002 Laser interstitial thermotherapy (LITT) monitoring using high-resolution digital mammography: theory and experimental studies *Phys. Med. Biol.* **47** 2987–99

Ntziachristos V, Yodh A G, Schnall M and Chance B 2000 Concurrent MRI and diffuse optical tomography of breast after indocyanine green enhancement *Proc. Natl Acad. Sci.* **97** 2767–72

O'Leary M 1996 Imaging with diffuse photon density waves *Dissertation in Physics* University of Pennsylvania

O'Leary M A, Boas D A, Chance B and Yodh A G 1995 Experimental images of heterogeneous turbid media by frequency-domain diffusing-photon tomography *Opt. Lett.* **20** 426–8

Ostermeyer M R and Jacques S L 1997 Perturbation theory for diffuse light transport in complex biological tissues *J. Opt. Soc. Am.* A **14** 255–61

Pearce J and Thomsen S 1995 Rate process analysis of thermal damage *Optical-Thermal Responses of Laser-Irradiated Tissue* ed A J Welch and M J C van Gemert (New York: Plenum)

Puccini S, Bar N K, Bublat M, Kahn T and Busse H 2003 Simulations of thermal tissue coagulation and their value for the planning and monitoring of laser-induced interstitial thermotherapy (LITT) *Magn. Reson. Med.* **49** 351–62

Ritz J P, Roggan A, Isbert C, Muller G, Buhr H J and Germer C T 2001 Optical properties of native and coagulated porcine liver tissue between 400 and 2400 nm *Lasers Surg. Med.* **29** 205–12

Roggan A, Ritz J P, Knappe V, Germer C T, Isbert C, Schadel D and Muller G 2001 Radiation planning for thermal laser treatment *Med. Laser Appl.* **16** 65–72

Terenji A, Willmann S, Osterholz J, Hering P and Schwarzmaier H J 2005 Measurement of the coagulation dynamics of bovine liver using the modified microscopic Beer–Lambert law *Lasers Surg. Med.* **36** 365–70

Verhey J F, Mohammed Y, Ludwig A and Giese K 2003 Implementation of a practical model for light and heat distribution using laser-induced thermotherapy near to a large vessel *Phys. Med. Biol.* **48** 3595–610

Whelan W M, Chin L C L, Davidson S R H and Vitkin I A 2005 A novel strategy for monitoring laser thermal therapy based on changes in optothermal properties of heated tissues *Int. J. Thermophys.* **26** 233–41

Whelan W M, Wyman D R and Wilson B C 1995 Investigations of large vessel cooling during interstitial laser heating *Med. Phys.* **22** 105–15